

Robust spatial memory maps encoded in networks with transient connections

Andrey Babichev¹, Dmitriy Morozov² and Yuri Dabaghian^{1*},

¹*Department of Computational and Applied Mathematics,
Rice University, Houston, TX 77005, USA*

²*Lawrence Berkeley National Laboratory,
Berkeley, CA 94720, USA*

**e-mail: dabaghian@gmail.com*

(Dated: November 16, 2018)

Abstract. The spiking activity of principal cells in mammalian hippocampus encodes an internalized neuronal representation of the ambient space—a cognitive map. Once learned, such a map enables the animal to navigate a given environment for a long period. However, the neuronal substrate that produces this map remains transient: the synaptic connections in the hippocampus and in the downstream neuronal networks never cease to form and to deteriorate at a rapid rate. How can the brain maintain a robust, reliable representation of space using a network that constantly changes its architecture? Here, we demonstrate, using novel Algebraic Topology techniques, that cognitive maps stability is a generic, emergent phenomenon. The model allows evaluating the effect produced by specific physiological parameters, e.g., the distribution of connections' decay times, on the properties of the cognitive map as a whole. It also points out that spatial memory deterioration caused by weakening or excessive loss of the synaptic connections may be compensated by simulating the neuronal activity. Lastly, the model explicates functional importance of the complementary learning systems for processing spatial information at different levels of spatiotemporal granularity, by establishing three complementary timescales at which spatial information unfolds. Thus, the model provides a principal insight into how can the brain develop a reliable representation of the world, learn and retain memories despite complex plasticity of the underlying networks and allows studying how instabilities and memory deterioration mechanisms may affect learning process.

Significance Statement. We explain how reliable representations of the world can emerge in networks with transient synaptic architectures. We study properties of the hippocampal cognitive map produced by place cell assemblies that recycle at the working memory timescale and demonstrate that the resulting “transient” network can represent the topology of the environment. We show that 1) this is a generic phenomenon, implementable via different mechanisms; 2) that deterioration of the memory map caused by excessive loss of the synaptic connections may be compensated by simulating the neuronal activity in the hippocampal network; 3) evaluate the effect produced by specific physiological parameters, e.g., the distribution of connections' decay times; 4) explicate three complementary timescales at which spatial information is processed in the brain.

I. INTRODUCTION

Functioning of the biological networks relies on synaptic and structural plasticity processes taking place at various spatiotemporal timescales [1–3]. For example, the so-called place cells in mammalian hippocampus learn to spike within specific locations of a new environment (their respective place fields) in a matter of minutes and then exhibit slow tuning of their firing rates for weeks [4–6]. The synaptic architecture of the hippocampal network constantly changes due to formation, adaptation and pruning of the synaptic connections via fast and slow plasticity mechanisms. In particular, detailed analyses of spike time statistics suggest that the place cells group into transient “assemblies” that may appear and disappear at working and intermediate memory timescales [7, 8].

The fact that the hippocampal network has a dynamic synaptic architecture poses a principal question: how can a rapidly rewiring network produce and sustain a stable cognitive map? How can it provide the downstream networks with stable spatial information? In the following, we address this question by modeling a population of dynamical place cell assemblies and studying the effect produced by the network’s transience on the large-scale representation of space, using algebraic topology tools. In particular, we demonstrate that despite rapid changes in its synaptic architecture, a transient cell assembly network can encode a stable large-scale topological map within a biologically plausible period.

II. THE TOPOLOGICAL MODEL

General outline. Our model of the hippocampal network is based on a schematic representation of the information provided by a population of spiking place cells in a given environment [9–12]. First, a group of coactive place cells, c_0, c_1, \dots, c_n is represented by an abstract simplex $\sigma = [c_0, c_1, \dots, c_n]$ —a basic object from algebraic topology that may be viewed geometrically as a n -dimensional tetrahedron with $n + 1$ vertexes (see Methods). Due to spatial tuning of the place cell activity, each individual coactivity simplex may also be viewed as a representation of the spatial overlap between the corresponding place fields. Together, the full collection of such simplexes forms a simplicial “coactivity” complex \mathcal{T} that represents spatial connectivity among the place fields that cover the environment \mathcal{E} —the place field map $M_{\mathcal{E}}$ (see Methods).

The formation of the coactivity complex represents the process of accumulating the topological information supplied by the place cell activity. At the beginning of navigation, when a few coactive place cells had time to fire, the complex $\mathcal{T}(M_{\mathcal{E}})$ contains a few simplexes that (typically) form several disconnected agglomerates (subcomplexes of \mathcal{T}), riddled with holes. Biologically, those may be viewed as fragments and gaps of the emerging cognitive map (Fig. 1A). If the parameters of spiking activity fall within the biological range of values, then, as more and more instances of coactivity are produced, the coactivity complex $\mathcal{T}(M_{\mathcal{E}})$ grows and eventually saturates, assuming a shape that is topologically equivalent to the shape of the navigated environment.

Mathematically, the topological structure of a steadily growing coactivity complex can be described using persistent homology theory methods [14, 15]. In particular, this theory allows detecting topological loops in $\mathcal{T}(M_{\mathcal{E}})$ (i.e., closed chains of simplexes identified up to topological equivalence [16]), on a moment-by-moment basis (Fig. 1B). Such loops provide a convenient semantics for describing how the shape of $\mathcal{T}(M_{\mathcal{E}})$ unfolds in time. For example, the number of inequivalent topological loops that can be contracted to a zero-dimensional vertex defines the number of the connected components in $\mathcal{T}(M_{\mathcal{E}})$; the number of loops that contract to a one-dimensional chain of links defines the number of holes and so forth. In the literature (see, e.g., [17]), the number of k -

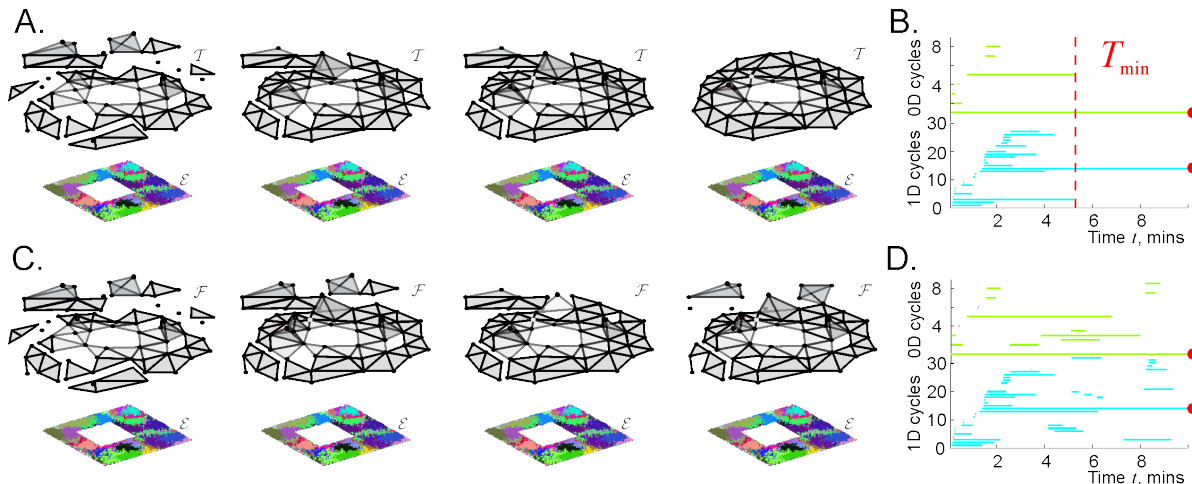


FIG. 1: Topological structure of the perennial and decaying coactivity complexes. A: Simulated place field map $M_{\mathcal{E}}$ of a small planar environment \mathcal{E} with a square hole in the middle (see Methods). Four consecutive snapshots illustrate the temporal dynamics of the coactivity complex: at the early stages of navigation the complex is small and fragmented, but as the topological information accumulates, the transient topological loops disappear, yielding a stable topological shape that is equivalent to the shape of the underlying environment. B: The timelines of topological loops in a steadily growing simplicial complex computed using persistent homology methods: the timelines of disconnected pieces (0D loops) are shown by light-blue lines and the timelines of one-dimensional holes (1D loops) are light-green. Most loops are spurious, i.e., correspond to accidental, short-lasting structures in $\mathcal{T}(M_{\mathcal{E}})$. The persistent topological loops (marked by red dots) represent physical features of the environment \mathcal{E} , i.e., its main connected component and the central hole. The time T_{\min} required to eliminate the spurious loops can serve as a theoretical estimate of the minimal time needed to learn path connectivity of the environment. C: If the simplexes may not only appear but also disappear, then the structure of the resulting “flickering” coactivity complex $\mathcal{F}(M_{\mathcal{E}})$ may never saturate. D: The timelines of the topological loops in such complex may remain interrupted by opening and closing topological gaps produced by decays and reinstatements of its simplexes.

dimensional topological loops in a space X is referred to as its k -th Betti number, $b_k(X)$, and the list of all Betti numbers defines the topological barcode, $\mathfrak{b}(X) = (b_0(X), b_1(X), \dots)$, that specifies the topological shape of X . For example, the simply connected, square environment \mathcal{E} with a single hole in the middle (Fig. 1A and Methods) has the Betti numbers $b_0(\mathcal{E}) = b_1(\mathcal{E}) = 1$, $b_{k>1}(\mathcal{E}) = 0$, and hence its topological barcode is $\mathfrak{b}(\mathcal{E}) = (1, 1, 0, 0, \dots)$.

The construction of the coactivity complexes may be adopted to reflect physiological aspects of the hippocampal network. For example, the simplexes of the coactivity complex may represent not just arbitrary combinations of coactive cells, but the actual, physiological neuronal assemblies—groups of cells that jointly elicit spiking activity in the downstream neurons. As mentioned in the introduction, these assemblies are unstable, transient structures that are recycled, according to different estimates, at the timescale between minutes to hundreds of milliseconds [7, 8]. In order to represent this transience, the coactivity complex has to acquire a qualitatively different dynamics: its simplexes should be allowed to appear and to disappear, i.e., “flicker,” following the appearances and disappearances of the corresponding cell assemblies. As a result, certain parts of the coactivity complex may inflate, while others may shrink, at different rates and in various sequences (Fig. 1C). The topological structure of such a “flickering” coactivity complex $\mathcal{F}(M_{\mathcal{E}})$ cannot, in general, be described using ordinary persistent homology theory methods (Fig. 1D), and requires a different mathematical apparatus—Zigzag persistent homology theory, outlined in the

Methods section and in [18–20].

Implementation. An efficient implementation of the coactivity complex is based on a classical “cognitive graph” model of the hippocampal network [21–23]. In this model, each active place cell c_i corresponds to a vertex v_i of graph \mathcal{G} , and the connections between pairs of cells (physiological or functional) are represented by the links $\zeta_{ij}^2 = [v_i, v_j]$ of \mathcal{G} . The assemblies of place cells c_1, c_2, \dots, c_n (“synaptically interconnected networks” in terminology of [8]) can then be naturally interpreted as fully interconnected subgraphs between the corresponding vertexes, i.e., as the maximal cliques $\zeta = [v_1, v_2, \dots, v_n]$ of \mathcal{G} [12, 13]. The connection with the topological model described above comes from the observation that cliques, as combinatorial objects, can be viewed as simplexes spanned by the same sets of vertexes. In other words, the collection of cliques of any graph G defines the so-called clique complex $\Sigma(G)$ [24], and hence the set of the coactivity cliques of \mathcal{G} can be viewed as the coactivity complex associated with the cognitive graph model. Such a complex effectively accumulates the information about place cell coactivity at various timescales, capturing the correct topology of planar [9–12] and voluminous [13] environments within minutes, which provides a suitable ground for constructing a “flickering complex” model for the network of dynamical cell assemblies. Specifically, one can use a coactivity graph \mathcal{G} with appearing and disappearing (flickering) links, and evaluate the topological shape of the corresponding flickering coactivity complex, using Zigzag persistent homology theory techniques. This constitutes a simple phenomenological model that connects the information provided by individual dynamical place cell assemblies and their physiological properties (e.g., the rate of their transience) to the structure of the large-scale topological maps encoded by the cell assembly network as a whole.

The model discussed below is implemented under the following principal assumptions.

I. *Decay of the synaptic connections.* A simple description of a transient network can be given in terms of the probabilities of the links’ appearances and disappearances at a given moment. For the latter, we adopt a basic “decay” model, in which an existing link ζ_{ij}^2 between cells c_i and c_j can disappear with the probability

$$p_{ij}(t) = \frac{1}{\tau_{ij}} e^{-t/\tau_{ij}},$$

where the time t is counted from the moment of the link’s last appearance and the parameter τ_{ij} defines its mean decay time. The decay times of the higher order cliques in the coactivity graph (i.e., of the higher order cell assemblies in the hippocampal network) are then defined by the corresponding link’s half-lives.

In a physiological cell assembly network, the decay times τ_{ij} should be distributed around a certain mean τ with a certain statistical variance [25]. However, in order to simplify the current model and to facilitate the interpretation of its outcomes, we attribute a single value $\tau_{ij} = \tau$ to all links in \mathcal{G} and use a unified distribution

$$p_0(t) = \frac{1}{\tau} e^{-t/\tau}, \quad (1)$$

to describe the deterioration of all synaptic connections within all cell assemblies. Thus, τ will be the only parameter that describes the decay of the synaptic connections in the model. We will therefore use the notations \mathcal{G}_τ and \mathcal{F}_τ to refer, respectively, to the flickering coactivity graph with decaying connections and to the resulting flickering clique coactivity complex with decaying simplexes.

II. *Appearances and rejuvenations of the synaptic connections.* We will assume that a connection ζ_{ij}^2 in the graph \mathcal{G} appears if the cells c_i and c_j become active within a $w = 1/4$ second period (biologically, this corresponds to consecutive periods of the θ -rhythm [10, 26]). The subsequent

coactivities of the pair $[c_i, c_j]$ either reinstate the link ζ_{ij}^2 (if it has disappeared by that moment) or rejuvenates it (i.e., its decay restarts). As a result, the links' actual or *effective* mean lifetime τ_e may differ from the proper decay time τ , which defines the expected lifetime of an unperturbed connection. Indeed, if the connection ζ_{ij}^2 that appeared at a moment t_1 does not disappear by the moment t_2 when the pair of cells $[c_i, c_j]$ reactivates, then its expected lifetime becomes $t_2 - t_1 + \tau$. If it does not decay before being “rejuvenated” again at a later moment t_3 , then its expected lifetime is $t_3 - t_1 + \tau$ and so forth. Notice however, that since place cells' spiking in learned environments is stable [27], the vertexes in the coactivity complex \mathcal{F}_τ appear with the first activation of the corresponding place cells and then never disappear.

III. *Fixed geometric parameters.* The series of instances at which a given combination of cells may become active is defined by the geometry of the place field map $M_\mathcal{E}$ and by the times of the rat's visits into the locations where the corresponding place fields overlap [28, 29]. In order to focus on the dependence of the topology of $\mathcal{F}_\tau(M_\mathcal{E})$ on the links' decay time, we selected a specific trajectory $\gamma(t)$ and a particular place field map $M_\mathcal{E}$ that induces a coactivity complex with correct topology in the “perennial” ($\tau = \infty$) limit [9, 10], and studied how the dynamics of the Betti numbers $b_k(\mathcal{F}_\tau(M_\mathcal{E}))$ depends on τ . In the following, we will therefore omit references to the place field map in the notations of the coactivity graph or the coactivity complex, and write simply \mathcal{G}_τ and \mathcal{F}_τ .

IV. *Restricted dimensionality.* Lastly, we note that although the coactivity complex is multidimensional [12], for a topological description of a planar environment it suffices to consider only the two-dimensional skeleton of \mathcal{F}_τ , i.e., the collection of second (ζ^2) and third (ζ^3) order connections (i.e., second or third order cliques of \mathcal{G}_τ or two- or three-vertex simplexes of \mathcal{F}_τ). Thus, in the following we will compute the coactive pairs and triples of the simulated neurons in order to study the topological properties of \mathcal{F}_τ as function of τ .

A priori, one would expect that if τ is too small, then the flickering complex \mathcal{F}_τ deteriorates too rapidly to produce a stable topological representation of the environment. In contrast, if τ is too large, then the effect of synaptic deterioration will not be significant. Thus, our goal will be to identify just how rapidly the coactivity simplexes can recycle while preserving the net topological structure of \mathcal{F}_τ . Physiologically, this will define how rapidly the hippocampal cell assemblies can rewire without jeopardizing the integrity of the topological map of the environment.

III. RESULTS

To start the simulations, we reasoned that in order for the flickering complex \mathcal{F}_τ to accumulate a sufficient number of simplexes and to capture the topology of the environment, its simplexes should not disappear between two consecutive coactivities of the corresponding cell groups. In other words, the characteristic lifetime of the links of the coactivity graph should exceed the typical interval between two consecutive activations of the corresponding cell pairs. In the simulated map, a typical link ζ^2 in the connectivity graph \mathcal{G} activates about $\langle n_2 \rangle = 50$ times during the $T_{tot} = 25$ min navigation period, i.e., the mean activation frequency is $f_2 \approx 1/30$ Hz (Fig. 2). Hence, in order to make room for the rejuvenation effects, we first tested the decay time of $\tau = 100$ secs, which is about three times longer than the inter-activity period and by an order of magnitude smaller than the total navigation time $\tau \approx T_{tot}/15$.

The histogram of the time intervals between the consecutive births and deaths of the links, $\Delta t_{\zeta_i^2} = t_{\zeta_i^2}^{(d_i)} - t_{\zeta_i^2}^{(b_i)}$, where the index i enumerates the birth (b_i) and the death (d_i) events, shown on Fig. 3A. First, we observe that the distribution of the link's effective lifetimes of both the two- and three-vertex connections has a bimodal shape. The relatively short ($\Delta t \leq 10\tau$) lifetimes

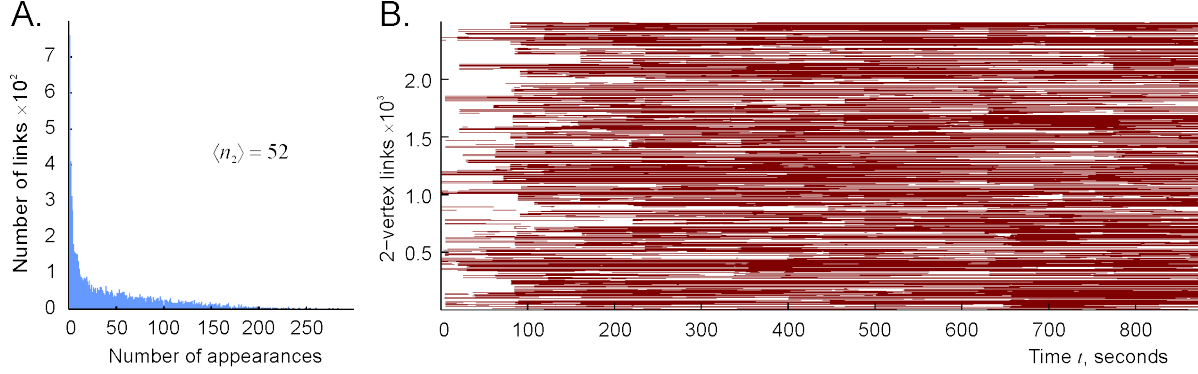


FIG. 2: **Time course of pairwise coactivity.** A: Histogram of the number of times that a given connection ζ^2 activates, computed for the place field map illustrated on Fig. 1 (for the corresponding occupancy map, see Methods). On average, a connection is activated about 50 times over the 25 min navigation period, i.e., once every 30 secs, although most links activate only a few times and some of them appear hundreds of times. B: Timelines of the links in the coactivity graph.

are exponentially distributed, implying that these connections are short-lived (the mode of the exponential distribution vanishes) and may be characterized by the effective decay times $\tau_e^{(2)}$ (links) that is about twice higher than τ and $\tau_e^{(3)}$ (triple connections) that is approximately equal to τ (Fig. 2). On the other hand, the bulging tails of the distributions shown on Fig. 3A,B represent an emergent population of long-lived pair and triple connections, i.e., a set of “survivor” simplexes that persist throughout almost the entire navigation period ($\Delta t_\zeta \approx T_{tot}$). Thus, the net structure of the lifetimes’ statistics suggests that the coactivity complex contains a stable “core” formed by a population of surviving simplexes, enveloped by a population of rapidly recycling, “fluttering,” simplexes.

The *mean* lifetime of each individual link, averaged over all the appearances across the entire navigation period, $\Delta t_{\zeta^2} = \langle t_{\zeta^2}^{(d_i)} - t_{\zeta^2}^{(b_i)} \rangle_i$, can be approximated by a lognormal distribution with the mode $m_2 \approx 4$ mins (Fig. 3C), which corresponds to the mean lifetime of the “fluttering” connections (Fig. 3A). Similarly, a typical third-order simplex appears for about two mins (Fig. 3C), as suggested by the mean of the distribution shown on Fig. 3B. Thus, on average, both the coactivity graph \mathcal{G}_τ and the corresponding coactivity complex \mathcal{F}_τ exhibit persistent structures, despite rapid flickering of the individual connections.

The rejuvenation of simplexes also affects the frequency of their (dis)appearances. As shown on Fig. 3E,F, a typical link and a typical third order connection disappear about 4 – 5 times during the navigation period, which is by an order of magnitude less than the links’ activation rate (Fig. 3B). Thus, a typical simplex rejuvenates about 10 times before getting a chance to decay. The histograms of the net lifetimes, i.e., of the total time that a given link or a clique spends in existence ($\Delta T_\zeta = \sum_i \Delta t_{\zeta,i}$) shown on Fig. 3G,H exhibit an even more salient contribution of the survivor simplexes. Note that the average net lifetime is approximately equal to the product of the mean effective lifetime and the mean number of appearances, $\Delta T_{e,\zeta} \approx n_{e,\zeta} \tau_{e,\zeta}$, as expected.

Dynamics of the flickering coactivity complexes. How does the decay of the connections affect the net structure of the flickering complex \mathcal{F}_τ ? As shown on Fig. 4A, the numbers of links $N_2(t)$ and of the triple connections $N_3(t)$ rapidly grow at the onset of the navigation and begin to saturate in about $t_s \approx 4$ mins (i.e., by the time when a typical link had time to make an appearance), reaching their respective asymptotic values in $t_a \approx 7$ mins. To put the size of the resulting flickering complex into a perspective, note that the number of simplexes in a decaying complex $\mathcal{F}_{\tau < \infty}$ can

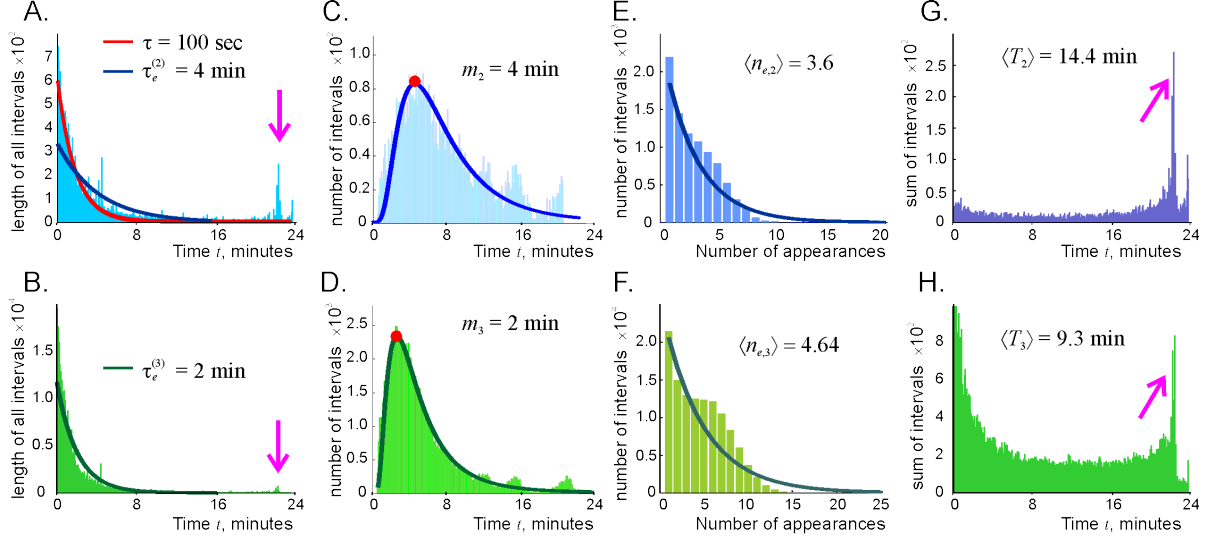


FIG. 3: Connection dynamics. A: The histogram of the time intervals between the consecutive births and deaths of the links, $\Delta t_{S_2,i} = t_{S_2}^{(d_i)} - t_{S_2}^{(b_i)}$, where the index i enumerates the birth (b_i) and the death (d_i) events. The mean of the exponential that fits the left side of the histogram (dark-blue line) is shown at the top of the panel. The pink arrow points at the population of the “survivor” links. The red line marks the distribution (1). B: Similar histogram for the third order simplexes. The histograms of the lifetimes averaged over all the instances of a given simplexes’ appearances $\Delta t_{S_2} = \langle t_{S_2}^{(d_i)} - t_{S_2}^{(b_i)} \rangle_i$ (panel C) and $\Delta t_{S_3} = \langle t_{S_3}^{(d_i)} - t_{S_3}^{(b_i)} \rangle_i$ (panel D). The modes of the resulting lognormal distributions (solid lines), m_2 and m_3 , correspond to the means shown on panels A and B. The histograms of the number of times the link and the triple connections activate during the navigation period are shown on the panels E and F. The exponential fits are shown by solid lines, with the means shown at the top of the panels. The distributions of total existence times for the second (panel G) and third (panel H) order simplexes, with the averages that are approximately equal to the product of the mean effective lifetime and the mean number of appearances, $\Delta T_{e,S} \approx n_{e,S} \tau_{e,S}$.

never exceed the number of simplexes that would have existed in absence of link decay, i.e., in the “perennial” coactivity complex, $\mathcal{F}_\infty \equiv \mathcal{T}$. Thus, the size of \mathcal{F}_τ can be characterized by the proportion of simplexes that happened to be actualized at that moment. As illustrated on Fig. 4A, these numbers fluctuate around 60% for the second order simplexes and around 40% for the third order simplexes, with the relative variances $\Delta N_2/N_2 \approx 12\%$ and $\Delta N_3/N_3 \approx 17\%$ respectively. In other words, the perennial coactivity complex $\mathcal{F}_\infty(t)$ loses about a half of its size due to the flickering of the simplexes, and fluctuates within about 15% margins from the mean.

To quantify the changes in the complexes’ structure as a function of time, we evaluated the number of two- and three-vertex simplexes that are present at a given moment of time t_i , but are missing at a later moment t_j , normalized by the size of $\mathcal{F}_\tau(t_i)$, i.e., $d_{ij}^{(k)} = N_k(\mathcal{F}_\tau(t_i) \setminus \mathcal{F}_\tau(t_j))/N_k(\mathcal{F}_\tau(t_i))$, $k = 2, 3$. As shown on Fig. 4B, these numbers, which we refer to, respectively, as the second and third asymmetric distances between $\mathcal{F}_\tau(t_i)$ and $\mathcal{F}_\tau(t_j)$, rapidly grow as a function of temporal separation $|t_i - t_j|$. In fact, after a τ_e -period, the difference between $\mathcal{F}_\tau(t_i)$ and $\mathcal{F}_\tau(t_j)$ becomes comparable to the sizes of either $\mathcal{F}_\tau(t_i)$ or $\mathcal{F}_\tau(t_j)$, which implies that the pool of simplexes in the simplicial complex is replenished at a τ_e -timescale. However, the shape of the coactivity complex changes slowly: Fig. 4C demonstrates that nearly 100% of the connections are shared at two consecutive moments, i.e., the changes in flickering complex from one moment of time to the next are marginal. As an additional illustration, we also computed the numbers of connections shared by the coactivity complex at a moment when \mathcal{F}_τ is inflated (about $t_* = 9$ mins, when a particularly

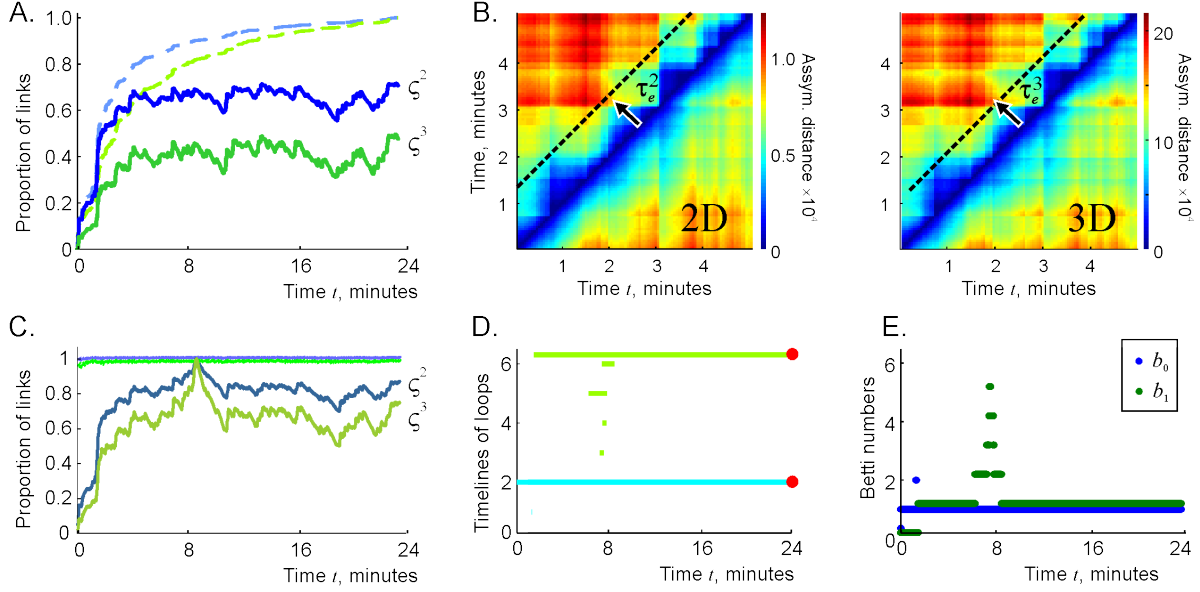


FIG. 4: Dynamics of the flickering complex. A: The number of links $N_2(t)$ in the flickering complex $\mathcal{F}_{100}(t)$ (blue trace) compared to the number of links in the perennial complex $\mathcal{F}_\infty(t)$ (dashed light-blue trace). The corresponding numbers of triple connections $N_3(t)$ are shown by the green and the dashed light-green traces, respectively. B: The matrix of asymmetric distances $d_{ij}^{(2)}$ and $d_{ij}^{(3)}$ (note the difference in scales shown by the color bars), computed over a five minutes time interval. The changes in the coactivity complex accumulate at the τ_e timescale. C: The proportions of second and third order connections shared by the coactivity complexes at the consecutive moments, computed for links (top light-green line) and for the triple connections (top light-blue line) closely follow the 100% mark, which implies that $\mathcal{F}_\tau(t)$ deforms slowly. The numbers of connections present at a moment of time when the coactivity complex is inflated ($t_* \approx 9$ min) that are also present at another moment t , $N_k(\mathcal{F}_\tau(t_*) \cap \mathcal{F}_\tau(t))$, fluctuate around $\sim 80\%$ for links ($k = 2$, blue trace) and $\sim 60\%$ for triple connections ($k = 3$, green trace), implying that the same set of connections is being reactivated. D: Timelines of 0D (light-blue) and 1D (light-green) topological loops in $\mathcal{F}_\tau(t)$ indicate a splash of topological fluctuations near the inflation time $t = 9$ mins. During other periods, $\mathcal{F}_\tau(t)$ contains only one persistent loop in each dimension. E: The instantaneous Betti numbers, $b_0(\mathcal{F}_\tau)$ and $b_1(\mathcal{F}_\tau)$ increase around $t_* = 9$ min, but retain their physical values $b_0(\mathcal{F}_\tau) = b_1(\mathcal{F}_\tau) = 1$ for the rest of the navigation period, which implies that, despite flickering-induced deformations, the topological shape of the coactivity complex remains stable during almost the entire navigation period.

large number of simplexes is simultaneously present) and other moments, when \mathcal{F}_τ is less bloated. The results shown on Fig. 4C indicate that the number of shared second and third order simplexes is respectively $N_2(\mathcal{F}_\tau(t_*) \cap \mathcal{F}_\tau(t)) \approx 82\%$ and $N_3(\mathcal{F}_\tau(t_*) \cap \mathcal{F}_\tau(t)) \approx 64\%$, i.e., that the recycling of the connections is due to partial reactivation of connections from the same pool.

Despite the rapid recycling of the individual simplexes, the large-scale topological characteristics of the flickering complex remain relatively stable. As demonstrated on Fig. 4D, after the initial stabilization period of about two minutes (which biologically may be interpreted as the initial learning period), \mathcal{F}_τ contains only one zero-dimensional and a single one-dimensional topological loop—as the simulated environment \mathcal{E} . Some topological fluctuations appear around $t \approx 9$ mins, as indicated by an outburst of short-lived spurious loops, most of which last for about a minute or less. After this period, the first two Betti numbers of \mathcal{F}_τ retain their physical values $b_0(\mathcal{F}_\tau) = b_1(\mathcal{F}_\tau) = 1$ (Fig. 4E). Since Zigzag homology theory allows tracing individual loops in \mathcal{F}_τ continuously across time, these persistent topological loops can be viewed as ongoing represen-

tations of the simply connected environment \mathcal{E} and of the physical hole in it. Thus, the coactivity complex \mathcal{F}_τ preserves, for the most time, not only its approximate size, but also its topological shape—despite transience at the “microscale”, i.e., at the individual simplex level.

Physiologically, these results indicate that the large-scale topological information outlives the network’s connections: although about a half of the functional links in the discussed case rewire within a τ_e -period, the topological characteristics of the cognitive map encoded by the cell assembly network remain stable. In other words, a transient cell assembly network can encode stable topological characteristics of the ambient space, despite transience of the synaptic connections.

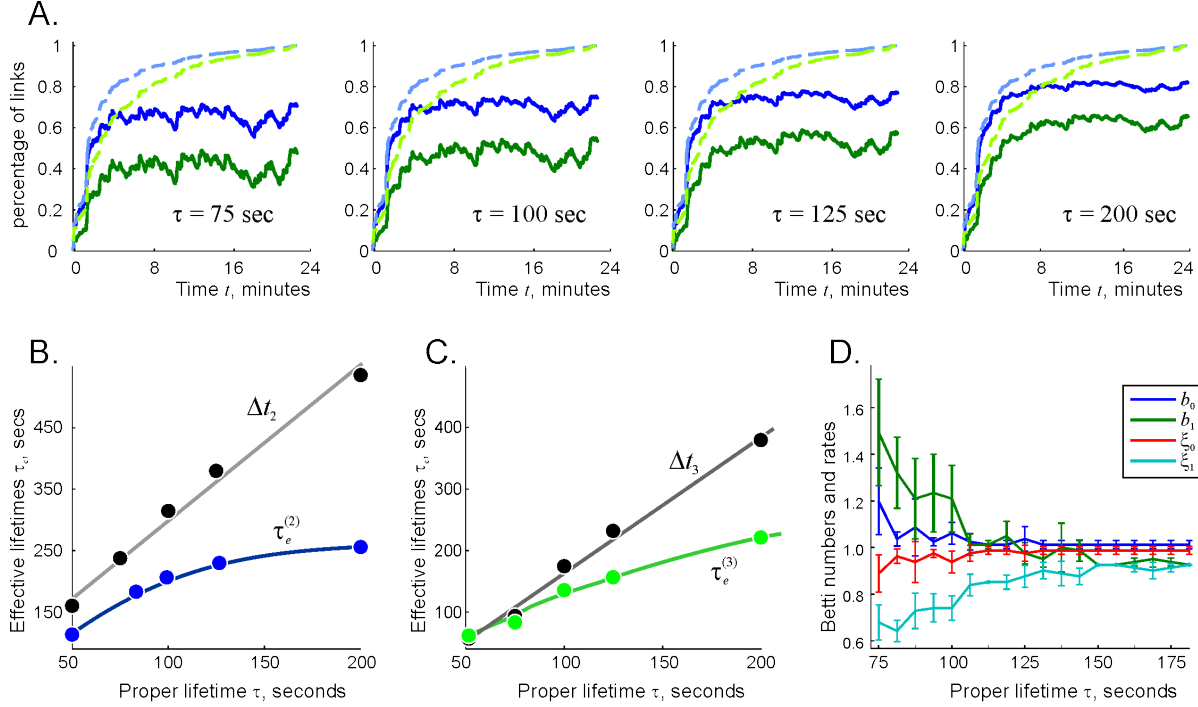


FIG. 5: τ -dependence of the functional connections and of the topological loops. A: The number of the two-vertex cliques ($N_2(\mathcal{F}_\tau, t)$, green trace) and the number of three-vertex cliques ($N_3(\mathcal{F}_\tau, t)$, blue trace) in the decaying complex, contrasted with the total number of two-vertex and three-vertex connections in the perennial complex across time ($N_2(\mathcal{F}_\infty, t)$ is shown by dashed light-green line and $N_3(\mathcal{F}_\infty, t)$ by light-blue line). The horizontal alignment of panels is used to emphasize increase in the asymptotic values $N_{2,3}(\mathcal{F}_\tau, t \gg \tau)$. B: The mean lifetimes of the “fluttering” links (i.e., the non-survivor links) in the coactivity complex are about twice longer than the proper link lifetimes, $\tau_e^{(2)} \approx 2\tau$ (blue line). The mean lifetimes of all the links in the coactivity complex (i.e., including the survivor, or “core” links) are about thrice longer than the proper lifetime, $\Delta t_{\mathcal{S}_2} \approx 3\tau$ (gray line). C: Same dependences are shown for the triple connections. The effective lifetimes of the short-lived triple connections are approximately equal to proper link lifetime, $\tau_e^{(3)} \approx \tau$. D: The dependence of the Betti numbers of the flickering complex, $b_k(\mathcal{F}_\tau)$, $k = 0, 1$ and the corresponding percentages of the successful trials $\xi_k(\mathcal{F}_\tau)$, on the proper decay time demonstrates that the topological fluctuations in \mathcal{F}_τ subside as τ increases.

Dependence on the proper decay time τ . Next, we investigated the topological stability for a set of proper decay times τ ranging from one to five minutes. As expected, the number of simplexes in the flickering complex increases with growing τ : in the studied map, the number of links raises from about 40% at $\tau = 75$ secs to just under 60% for $\tau = 200$ secs, whereas the number of the third order connections raises from 60% to about 80% (Fig. 5A). The distributions of the effective lifetimes for the short-lived (fluttering) connections retain their exponential shapes

(Fig. S1), with the means that are approximately proportional to the proper decay times, $\tau_e^{(2)} \approx 2\tau$ and $\tau_e^{(3)} \approx \tau$ (Fig. 5B,C). The contribution of the surviving simplexes also steadily grows with τ (Fig. S1); as a result, the net average lifetimes, computed for the entire population of simplexes, grow faster $\Delta t_{s_2} \approx 3\tau$ and $\Delta t_{s_3} \approx 2\tau$.

As τ increases, the Betti numbers rapidly reduce to their physical values, $b_0(\mathcal{F}_\tau) = b_1(\mathcal{F}_\tau) = 1$: the lower is the connection decay rate, the smaller are the topological fluctuations generated in the flickering complex (Fig. 5D and Fig. S2A,B). This is a natural result: since the ‘‘perennial’’ map \mathcal{F}_∞ converges to a stable, topologically correct shape in a matter of minutes, the longer the simplexes survive in the decaying case ($\tau < \infty$), the closer the topological barcode of \mathcal{F}_τ should be to the barcode of the environment \mathcal{E} . As shown on Fig. 5D, a stabilization of topological barcode is achieved around $\tau \sim 2$ mins. This value can also be naturally interpreted: for such τ , the rat moving at the mean speed of about 25 cm/sec has time to complete a circle around the central hole before a typical connection disappears, which allows the induced coactivity complex to capture this key feature of the environment and to contract the spurious topological loops. Note however, that this is only a qualitative argument since the expected lifetimes of over 63% of links is smaller than τ and the lifetimes of 15% of them live longer than 2τ .

Fixed connection lifetimes. To test how these results are affected by the spread of the link lifetimes, we investigated the case in which the lifetimes of all the links are fixed, i.e., the decay probability is defined by the function

$$p(t) = \begin{cases} 1 & \text{if } t = \tau \\ 0 & \text{if } t \neq \tau. \end{cases} \quad (2)$$

while keeping the other parameters of the model unchanged. The results shown on Fig. 6A demonstrate that due to the rejuvenation effects, the range of the effective lifetimes widens and becomes qualitatively similar to the histograms induced by the decay distribution (2). As before, there appear two distinct populations of links: the short-lived links whose lifetimes concentrate around the singular proper lifetime τ , and the ‘‘survivor’’ links, whose lifetimes approach T_{tot} .

However, the topological structure of the ‘‘fixed-lifetime’’ coactivity complex \mathcal{F}_τ^* differs dramatically from that of the decaying complex \mathcal{F}_τ . As shown on Fig. 6C, \mathcal{F}_τ^* contains a large number of short-lived, spurious topological loops even for the values of τ that reliably produce physical Betti numbers in the case of the exponentially distributed link lifetimes. For example, at $\tau = 100$ secs, the zeroth Betti number of \mathcal{F}_τ^* hovers at the average value of $\langle b_0 \rangle \approx 40$, reaching at times $b_0 \sim 100$, with nearly unchanged $b_1 = 1$, which indicates that at this decay rate, \mathcal{F}_τ^* brakes into a few dozens of disconnected, topologically contractible islets.

As the proper decay time increases, the population of survivor links grows and the disconnected pieces of \mathcal{F}_τ^* begin to pull together: at $\tau = 200$ secs, the Betti numbers $b_k(\mathcal{F}_\tau^*)$ retain their physical values for about a half of the time, yielding splashes of topological fluctuations during the other half (Fig. 6C,D).

These differences between the topological properties of \mathcal{F}_τ and \mathcal{F}_τ^* indicate that the tail of the exponential distribution (1), i.e., the statistical presence of long-lasting connections is crucial for producing the correct topology of the flickering complex. Physiologically, this implies that the statistical spread of the connections’ lifetimes plays important role: in absence of statistical variations, the dynamical cell assembly network fails to represent the topology of the environment.

Randomly flickering connections. These observations led us to another question: might the topology of the flickering complex be controlled by the shape of the lifetimes’ distribution and the sheer number of links present at a given moment, rather than the specific timing of the links’ appearance and disappearance? To test this hypothesis, we computed the number $n(t)$ of links in the

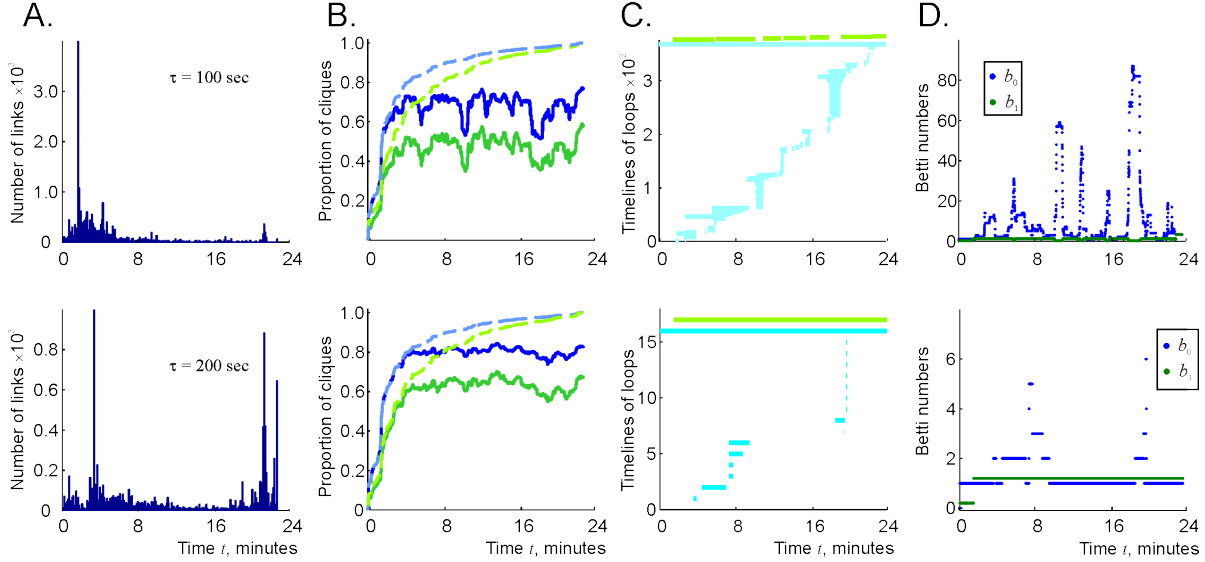


FIG. 6: Fixed connection lifetimes lead to topological instabilities. A: The effective timelines of links with the proper decay time of $\tau = 100$ secs (top) and $\tau = 200$ secs (bottom). The contribution of the links retaining the original, singular proper decay time ($\tau_e = \tau$) is manifested in the sharp solitary peaks on the left sides of the histograms. The values to the left of that peak are produced by the “boundary effect”: cutting the simulation at T_{tot} produces timelines shorter than τ . B: The distributions of the numbers of two- and three-vertex connections in (green and blue traces) vs. same numbers in the perennial complex $\mathcal{F}_\infty(t)$ (dashed lines) indicate that the number of instantiated connections in the case of the singular distribution (2) is higher than in the case of the distribution (1) (see Fig. 4A and Fig. 5A). As τ grows twofold (from 100 to 200 secs) the number of links $N_2(\mathcal{F}_\tau^*)$ grows by 40% and the number of triple connections $N_3(\mathcal{F}_\tau^*)$ grows by 30%. C: The timelines of 0D (light-blue) and 1D (light-green) topological loops in the $\tau = 100$ secs (top) and in the $\tau = 200$ secs (bottom) case. The former produces hundreds of short-lived, spurious loops, while in the latter case there is about a dozen of loops that persist for about 50% of the time. The behavior of the corresponding Betti numbers b_0 (blue) and b_1 (green) is shown on panel D.

decaying coactivity graph $\mathcal{G}_\tau(t)$ for $\tau = 100$ sec at every discrete moment of time t (see Methods), and randomly selected the same number of links from the maximal available pool, i.e., from the graph $\mathcal{G}_\infty(t)$ that would have formed by that moment without links’ decay (Fig. 7A). The collections of links randomly selected at consecutive moments of time can be viewed as instances of a stochastic connectivity graph $\mathcal{G}_r(t)$, i.e., as a graph whose links make random and instantaneous appearances and disappearances, in contrast with the decaying links of $\mathcal{G}_\tau(t)$ (compare Fig. 7B and Fig. 2B).

Surprisingly, the random and the decaying graphs $\mathcal{G}_r(t)$ and $\mathcal{G}_\tau(t)$, as well as their respective clique complexes $\mathcal{F}_r(t)$ and $\mathcal{F}_\tau(t)$ possess a number of similar topological properties. First, the histogram of the *net* lifetimes of the links in $\mathcal{G}_r(t)$ shown on Fig. 7C is bimodal, with an exponential part characterized by the mean $\langle T_2 \rangle = 124$ sec and a component representing a population of surviving connections, similar to the histograms shown on Fig. 3G,H. Second, the Betti numbers of the stochastic coactivity complex \mathcal{F}_r converge to the Betti numbers of the environment in about 3 mins—about as quickly as the Betti numbers of its decaying counterpart \mathcal{F}_τ (Fig. 7D). However, in contrast with \mathcal{F}_τ , \mathcal{F}_r keeps producing occasional fluctuations of one-dimensional spurious loops over the entire navigational period at a low rate (about 3% of the time, Fig. S3). Thus, the topological shapes of the random and the decaying coactivity complexes remain close. In other words, according to the model, the topological properties of the map encoded by a network with

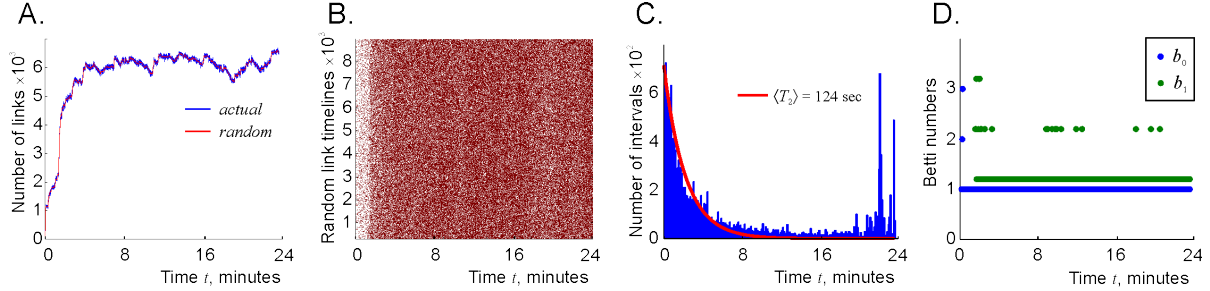


FIG. 7: **Stochastic complex.** A: The number of links in the stochastic coactivity graph $\mathcal{G}_r(t)$ (blue trace) is the same as in the decaying coactivity graph $\mathcal{G}_\tau(t)$ (red trace). B: The links of the stochastic coactivity graph $\mathcal{G}_r(t)$ make instantaneous appearances and disappearances. Compare this chart to the timelines of the links in the decaying coactivity graph $\mathcal{G}_\tau(t)$ shown on Fig. 2B. C: Histogram of the link’s net lifetimes in the stochastic graph indicates populations of short-lived and survivor links, similarly to the histogram shown on Fig. 3G. D: Betti numbers of the stochastic complex stabilize after the initial learning period of about four minutes, indicating the emergence of a stable topological shape of the simplicial complex with stochastically flickering simplexes.

randomly formed and pruned connections are similar to the properties of a map produced by a network with decaying connections, as long as the net probability of the links’ existence are same. In either case, rapidly rewiring connections do not preclude the appearance of a stable topological map.

Compensatory mechanisms. The turnover of memories (encoding new memories, integrating them into the existing frameworks, recycling old memories, consolidating the results, etc.) is based on adapting the synaptic connections across different brain regions [30]. In particular, these processes require a balanced contribution of both “learning” and “forgetting” components, i.e., forming and pruning the functional and/or physiological connections [31, 32]. The imbalances and pathological alterations in the corresponding synaptic mechanisms are observed in many neurodegenerative conditions, e.g., in the Alzheimer’s disease, which is known to affect spatial cognition [33]. However, interpreting the physiological meaning of these alterations is a highly nontrivial task, in particular because certain changes in neuronal activity may not be direct consequences of neurodegenerative pathologies. For example, it is believed that neuronal ensembles may increase the spiking rates of the active neurons in order to compensate for the reduced synaptic efficacies [34–40]. Such considerations motivate deep brain stimulation and other treatments that help to improve cognitive performance in animal models of Alzheimer’s diseases and in Alzheimer’s patients, by increasing the electrophysiological activity of hippocampal cells [41, 42].

Previous studies, carried out for the models of perennial cell assembly networks [43], provided a certain theoretical justification for these approaches. For example, it was demonstrated that a place cell ensemble that fails to produce a reliable topological map of the environment due to an insufficient number of active neurons might be forced to produce a correct map by increasing the active place cells’ firing rates. Similarly, the reduction in the firing rates or poor spatial selectivity of spiking may sometimes be compensated by increasing the number of active cells and so forth. Since the current model allows modeling networks with transient synaptic connections, we wondered whether it might point out other compensatory mechanisms, e.g., indicate a theoretical possibility to compensate for the reduced cell assemblies’ lifetimes by increasing the spiking activity of the place cells.

To that end, we varied the mean firing rate f and the number of cells N in the simulated place cell ensemble and studied the topological properties of the resulting coactivity complex as

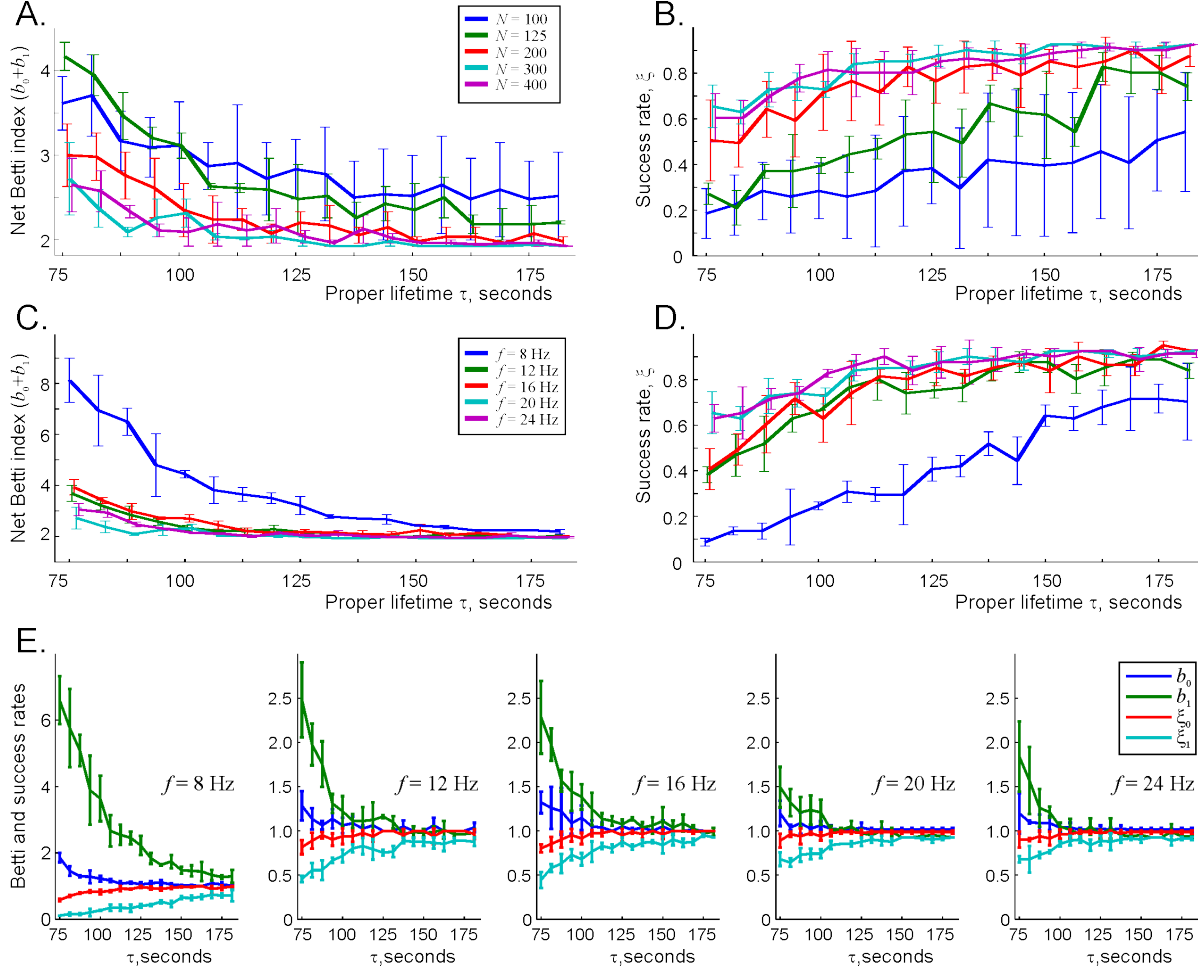


FIG. 8: Suppression of the topological fluctuations by increasing neuronal spiking activity. A: As the number of active cells increases, the number of spurious topological loops drops. To compactify the information, we use the sum of the first two Betti numbers, $b = (b_0 + b_1)$, which describes the total number of $0D$ and $1D$ loops as a function of decay rate τ , computed for several ensemble sizes. As the number of active cells with mean firing rate $f = 14$ Hz increases from $N = 100$ to $N = 400$ cells, the number of loops decrease from 3-4 (indicating at least one spurious loop in $0D$ or in $1D$) to the physical value $b_0(\mathcal{E}) + b_1(\mathcal{E}) = 2$. B: The proportion of trials—the success rate, ξ —in which the coactivity complex produces the correct signature, $b_k(\mathcal{F}_\tau) = b_k(\mathcal{E})$, as a function of the number of cells, N . Larger place cell ensembles tend to represent the topology of the environment more reliably. C: Sum of Betti numbers for different firing rates and $N=300$ cells. As the mean ensemble rate increases from $f = 8$ to $f = 24$ Hz, the spurious loops die out, i.e., the topological fluctuations in \mathcal{F}_τ are suppressed. D: The success rate ξ_k as a function of the decay rate τ , computed for a set of firing rates and $N = 300$. As before, the reliability of the map increases with the mean ensemble rate for the entire range of the proper decay times. E: Betti numbers $b_k(\mathcal{F}_\tau)$, $k = 0, 1$, converge to their physical values $b_k(\mathcal{E})$ faster and their respective success rates ξ_k grow more rapidly at higher firing rates.

a function of the links' proper half-life, τ . The results shown on Fig. 8 demonstrate that indeed, increasing neuronal activity helps to suppress topological fluctuations in the flickering coactivity complex for a wide range of the connections' decay times. Moreover, these changes also increase the proportion ξ of trials in which the place cell ensemble captures the correct signature of the environment.

Physiologically, these results indicate that recruiting additional active cells and/or boosting

place cell firing rates allows to compensate for an overly rapid deterioration of synaptic connections, i.e., increasing neuronal activity stabilizes the topological map. In particular, a higher responsiveness of the Betti numbers of the flickering coactivity complex to an increase of the mean firing rate (Fig. 8C,E). as compared to the number of active place cells (Fig. 8A) suggests that targeting the active neurons’ spiking may provide a better strategy for designing clinical stimulation methods.

IV. DISCUSSION

The formation and disbanding of dynamical place cell assemblies at the short- and intermediate-memory timescales enables rapid processing of the incoming information in the hippocampal network. Although many details of the underlying physiological mechanisms remain unknown, the schematic approach discussed above provides an instrument for exploring how the information provided by the individual cell assemblies combines into a large-scale spatial memory map and how this process depends on the physiological parameters of neuronal activity. In particular, the model demonstrates that a network with transient synaptic connections can successfully capture the topological characteristics of the environment.

Previously, we investigated this effect using an alternative model of transient cell assemblies, in which the connections were constructed by identifying the pool of cells that spike within a certain “coactivity window,” ϖ , and building the coactivity graph \mathcal{G}_ϖ by selecting the most frequently cofiring pairs of neurons [43]. The accumulation of topological information within each ϖ -period (physiologically, ϖ can be viewed as the time over which the downstream networks integrate place cell outputs), was then described using persistent homology theory techniques. The results indicate that if ϖ extends over 4–6 mins or more, the topological fluctuations in the flickering complex are suppressed and the topological shape of \mathcal{F}_ϖ becomes equivalent to the shape of the environment.

In the current model, enabled by the much more powerful Zigzag persistent homology theory [18–20], we employ an alternative approach, in which the links of the coactivity graph appear instantly following pairwise place cell coactivity events. Thus, in contrast with the model discussed in [43], the current model involves no accumulation of spiking information and no selection of the “winning” coactivity links, which one might hold responsible for stabilizing the shapes of the flickering coactivity complexes. Nevertheless, the “latency free” model demonstrates the same effect: the large-scale topological shapes of resulting coactivity complexes stabilize, given that the connections decay sufficiently slowly and have sufficiently broadly distributed lifetimes. The connections’ lifetimes required to achieve such stabilization are longer than in the input integration model ($\tau \approx 100$ sec vs. $\tau_\varpi \approx 10$ sec), which indicates that implementing a stable topological map in a physiological network with rapidly recycling functional connections may require integrating spiking information over an extended period and optimizing the network’s architecture over this information. However, the fact that stable topological maps can emerge in different types of transient networks (including stochastically flickering networks) suggests that this is a generic effect that may explain appearance of stable cognitive representations of the environment in different physiological neuronal networks with “plastic” synaptic connections. In other words, the emergence of stable topological maps may represent a common “umbrella” phenomenon that can be implemented via different physiological mechanisms.

In all cases, the model reveals three principal timescales of spatial information processing. First, the ongoing information about local spatial connectivity is rapidly processed at the working memory timescale, which physiologically corresponds to rapid forming and disbanding of the dynamical place cell assemblies in the hippocampal network. The large-scale characteris-

tics of space as described by the instantaneous Betti numbers unfold at the intermediate memory timescale, whereas at the long-term memory timescale the topological fluctuations average out, yielding stable, qualitative information about the environment. Thus, the model reaffirms functional importance of the complementary learning systems for processing spatial information at different timescales and at different levels of spatial granularity [30, 44, 45].

V. METHODS

Place cell spiking activity is modeled as a stationary temporal Poisson process with the maximal firing rate f_c localized in a place field centered at r_c ,

$$\lambda_c(r) = f_c e^{-\frac{(r-r_c)^2}{2s_c^2}}$$

where s_c defines the place field’s size [46]. An ensemble of N place cells is therefore defined by $3N$ independent parameters, which we consider as random variables drawn from the stationary distributions, characterized by a mean firing rate, f , and the mean place field size s , i.e., by a point (s, f, N) in a $3D$ parameter space. In addition, spiking is modulated by the θ -oscillations—a basic cycle of the extracellular local field potential (LFP) in the hippocampus, with the frequency of ~ 8 Hz [47]. We study an ensemble of $N = 300$ place cells, with the typical maximal firing rate $f = 14$ Hz and the typical place field size $s = 20$ cm.

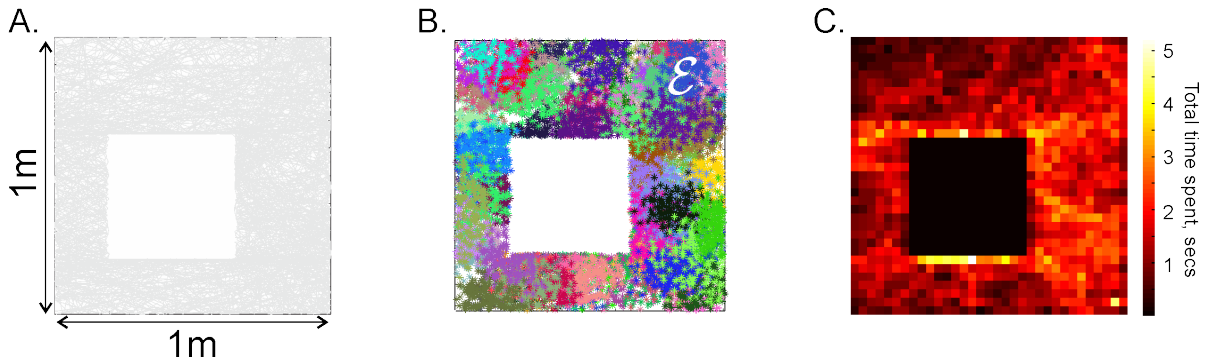


FIG. 9: **Simulated Environment.** A: The trajectory covers a small planar arena \mathcal{E} uniformly, without artificial circling or other ad hoc favoring of one segment of the environment over another. B: Simulated place field map $M_{\mathcal{E}}$. Clusters of dots of a particular color represent spikes produced by the corresponding place cells. C: A $2D$ histogram of the time spent by the animal in different locations—the occupancy map of \mathcal{E} .

Place cell coactivity. We consider a group of place cells c_0, \dots, c_k *coactive*, if they produce spikes within two consecutive θ -periods [10, 26]. As a result, the time interval $[0, T_{tot}]$ splits into $1/4$ sec long time bins that define the discrete time steps t_1, \dots, t_n, \dots , used throughout the text [12].

Simulated environment \mathcal{E} represents a small ($1m \times 1m$) square arena with a square hole in the middle, similar to the environments used in electrophysiological experiments [48]. Fig. 9 shows the simulated trajectory, the layout of the place fields in \mathcal{E} —the place field map $M_{\mathcal{E}}$, and the occupancy map. In [10] we demonstrated that different parts of the environment can be learned independently from one another. Thus, knowing how learning works in small spatial domains, one can “map out” environments of different geometric and topological complexity. In particular, considering small environment shown above is sufficient for establishing the main effect (stability of global maps in transient networks) in general case.

Simplicial complexes. We use simplexes and simplicial complexes to represent combinatorially the topology of the neural activity. An abstract *simplex* of dimensionality n is a set containing $n + 1$ elements. A subset of a simplex is called its *face*. A *simplicial complex* is a collection of simplexes closed under the face relation: if a simplex belongs to a simplicial complex, then so do all of its faces (Fig. 10).

In the constructions studied in this paper, our simplicial complexes consist of coactive place cells. If all cells $\{c_0, \dots, c_k\}$ are coactive within a given time window, then so is any subset of them, meaning coactive simplexes form a complex. In fact, because coactivity is defined for a pair of cells, our simplexes are precisely the cliques in the coactivity graph. A simplex $\{c_0, \dots, c_k\}$ is present if and only if all of its cells are pairwise coactive.

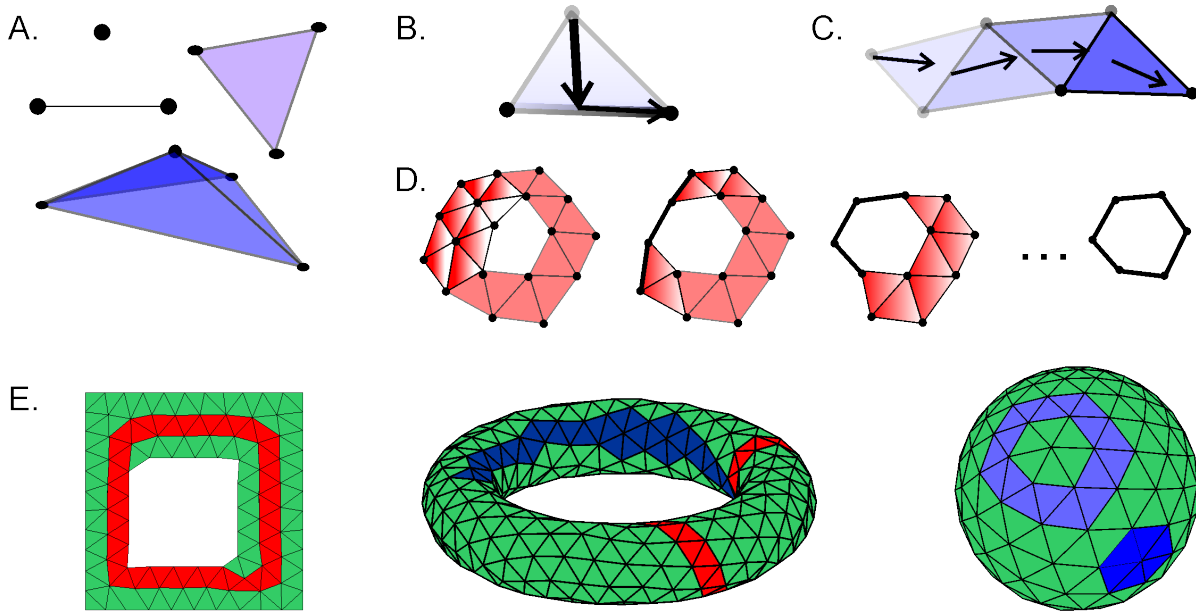


FIG. 10: Simplexes and simplicial complexes. A: A zero-dimensional (0D) simplex σ_i^0 corresponds to a point vertex v_i ; a one-dimensional (1D) simplex σ_{ij}^1 —to a link between two vertexes v_i and v_j ; a two-dimensional (2D) simplex σ_{ijk}^2 —to a filled triangle; a three-dimensional (3D) simplex σ_{ijkl}^3 —to a filled tetrahedron, etc. The n vertexes connected by the full set of 1D links form cliques, σ^n , of the corresponding order. B: A single simplex σ^n is a contractible figure, i.e., it can be collapsed into one of its facets σ^{n-1} , then to a facet of lower dimensionality σ^{n-2} and eventually to a point σ^0 . Shown is a triangle contracting onto its bottom edge and then to the right vertex. C: A linear chain of simplexes bordering each other at a common face is also contractible. The shade of the triangles constituting the chain defines the order in which the triangles can be contracted (the lighter is the triangle, the sooner it contracts) and the arrows indicate the direction of the contractions. D: If a chain of simplexes loops onto itself and encircles a gap in the middle, then it is not contractible. Collapsing the triangles on the sides of such a closed chain produces an equivalent closed loop, which, ultimately, can be reduced to a non-contractible 1D loop, but not to a 0D vertex (the hole in the middle prevents that). Topologically, the deformed loops are equivalent to one another, i.e., they should be viewed as deformations of the same topological loop. E: Three simplicial complexes: a complex shaped as the environment \mathcal{E} (see Fig. 1), a toroidal and a spherical complexes (figures obtained using MATLAB mesh generator [49]). Non-contractible topological loops are shown as closed chains of red triangles and contractible loops are shown in shades of blue.

In flickering clique complexes, certain pairwise connections may decay over time, while others appear as time progresses. The effect on the simplicial complex is that some simplexes are removed

from the complex, while others are added to it. So we get a sequence of “flickering complexes,” X_i , connected by alternating inclusions:

$$X_1 \subseteq X_2 \subseteq X_3 \supseteq X_4 \subseteq X_5 \supseteq \dots$$

Cycles, boundaries, and homology. A k -dimensional *chain* is a set of k -dimensional simplexes (Fig. 10) that can be combined with suitable coefficients. If the coefficients form an algebraic field, then the chains form a vector space. Here we use the simplest algebraic field \mathbb{Z}_2 , which consists of two Boolean values 0 and 1. A boundary of the simplex is the sum of its one-dimension-lower faces: $\partial_k\{c_0, \dots, c_k\} = \sum_{i=0}^k \{c_0, \dots, c_{i-1}, c_{i+1}, \dots, c_k\}$. The map extends linearly to the entire simplicial complex, X , mapping its k -dimensional chains to its $(k-1)$ -dimensional chains. The kernel of this map, i.e., all the chains without a boundary, is the set of *cycles* of the complex, denoted by $Z_k(X) = \ker \partial_k$. The image of ∂_{k+1} consists of the k -dimensional chains that are *boundaries* of some $(k+1)$ -dimensional chains, denoted by $B_k(X) = \text{im } \partial_{k+1}$.

Cycles count “ k -dimensional holes” in the complex. But not all such holes are independent of each other. We consider two cycles equivalent, or *homologous*, if they differ by a boundary. Algebraically, one can verify that boundaries themselves have no boundaries, $\partial_k \circ \partial_{k+1} = 0$. In other words, boundaries are cycles. This allows us to take a quotient, $H_k(X) = Z_k(X)/B_k(X)$, called the k -dimensional *homology* vector space. By definition, it considers two cycles equivalent, if their difference is a boundary of some $(k+1)$ -dimensional chain. The dimension of this vector space, called the k -th Betti number, $\beta_k(X) = \dim H_k(X)$, counts the number of independent holes in the topological space.

Zigzag persistent homology. Given the sequence of flickering complexes above, we compute homology of each one. Inclusions between complexes induce maps between the homology vector spaces: the homology class of a cycle in the smaller complex maps to the homology class of the same cycle in the larger complex. Accordingly, we get a sequence of homology vector spaces, connected by linear maps:

$$H_k(X_1) \rightarrow H_k(X_2) \rightarrow H_k(X_3) \leftarrow H_k(X_4) \rightarrow H_k(X_5) \leftarrow \dots$$

This sequence, called *zigzag persistent homology*, generalizes ordinary persistent homology [20], where all the maps between homology groups point in the same direction. It is this generalization to the alternating maps that allows us to handle the flickering complexes.

On the surface, zigzag persistent homology tracks how the Betti numbers of the flickering complexes change. But the maps that connect homology vector spaces provide extra information. It is possible to select a basis for each vector space in this sequence, so that the bases for adjacent vector spaces are compatible [18]. Specifically, we can select a collection of elements $\{z_i^j\}_j$ for each vector space $H_k(X_i)$, such that the non-zero elements form a basis for the homology vector space $H_k(X_i)$ — in other words, they represent a set of independent holes in X_i . Furthermore, such collections are compatible in the sense that adjacent basis elements map into each other: if we have a map $f : H_k(X_i) \rightarrow H_k(X_{i\pm 1})$, then $f(z_i^j) = z_{i\pm 1}^j$, if $z_i^j \neq 0$. The experiments in this paper use the algorithm of Carlsson et al. [19] to compute such compatible bases.

It follows that the sequence of homology vector spaces can be decomposed into a barcode, where each bar represents the part of the sequence, where a particular basis element is non-zero. The bars capture when independent holes appear in the flickering complex, how long they persist, and when they eventually disappear.

VI. ACKNOWLEDGMENTS

The work was supported by the NSF 1422438 grant and by the Houston Bioinformatics Endowment Fund.

VII. REFERENCES

- [1] Bi GQ, Poo MM (2001), Synaptic Modification by Correlated Activity: Hebb's Postulate Revisited, *Annu. Rev. Neurosci.* 24: 139-166.
- [2] Leuner B, Gould E (2010), Structural Plasticity and Hippocampal Function, *Annu. Rev. Psychol.* 61: 111-140.
- [3] Caroni P, Donato F, Muller D (2012), Structural plasticity upon learning: regulation and functions, *Nat Rev. Neurosci.*, 13: 478-490.
- [4] Best PJ, White AM, Minai A (2001), Spatial processing in the brain: the activity of hippocampal place cells, *Annu. Rev. Neurosci.* 24: 459-486.
- [5] Frank LM, Brown EN, Stanley GB (2006), Hippocampal and cortical place cell plasticity: implications for episodic memory, *Hippocampus* 16: 775-784.
- [6] Karlsson MP, Frank LM (2008), Network dynamics underlying the formation of sparse, informative representations in the hippocampus, *J Neurosci.* 28: 14271-14281.
- [7] Harris KD, Csicsvari J, Hirase H, Dragoi G, Buzsaki G (2003), Organization of cell assemblies in the hippocampus, *Nature* 424:552-556.
- [8] Buzsaki G (2010), Neural syntax: cell assemblies, synapsembles, and readers, *Neuron* 68: 362-385.
- [9] Dabaghian Y, Mmoli F, Frank L, Carlsson G (2012), A Topological Paradigm for Hippocampal Spatial Map Formation Using Persistent Homology, *PLoS Comput. Biol.* 8: e1002581.
- [10] Arai M, Brandt V, Dabaghian Y (2014), The Effects of Theta Precession on Spatial Learning and Simplicial Complex Dynamics in a Topological Model of the Hippocampal Spatial Map, *PLoS Comput. Biol.*, 10: e1003651.
- [11] Basso E, Arai M, Dabaghian Y (2016), Gamma Synchronization Influences Map Formation Time in a Topological Model of Spatial Learning *PLoS Comput. Biol.* 12: e1005114.
- [12] Babichev A, Ji D, Memoli F, Dabaghian Y (2016), A Topological Model of the Hippocampal Cell Assembly Network, *Front Comput. Neurosci.*:10.
- [13] Hoffman K, Babichev A, Dabaghian Y (2016), A model of topological mapping of space in bat hippocampus, *Hippocampus*: 26 (10), pp. 1345-1353.
- [14] Ghrist R (2008), Barcodes: The persistent topology of data, *Bulletin of the American Mathematical Society* 45: 61-75.
- [15] Zomorodian A, and Carlsson, G. (2005), Computing persistent homology, *Discrete and Computational Geometry* 33: 249-274.
- [16] Friedman G (2012) Survey Article: An elementary illustrated introduction to simplicial sets, *Rocky Mountain J Math*: 353-423.
- [17] Hatcher A (2002), *Algebraic topology*, Cambridge; New York: Cambridge University Press.
- [18] Carlsson G, Silva Vd (2010), Zigzag Persistence, *Found. Comput. Math.* 10: 367-405.

- [19] Carlsson G, Silva Vd, Morozov D (2009), Zigzag persistent homology and real-valued functions. *Proceedings of the 25th annual symposium on Computational geometry*, Aarhus, Denmark: ACM. pp. 247-256.
- [20] Edelsbrunner H, Letscher, D., and Zomorodian, A. (2002), Topological Persistence and Simplification, *Discrete & Computational Geometry* 28: 511–533.
- [21] Muller RU, Stead M, Pach J (1996), The hippocampus as a cognitive graph, *J Gen. Physiol.* 107: 663-694.
- [22] Burgess N, O’Keefe J (1996), Cognitive graphs, resistive grids, and the hippocampal representation of space, *J Gen. Physiol.* 107: 659-662.
- [23] Babichev A, Cheng S, Dabaghian Y (2016), Topological schemas of cognitive maps and spatial learning, *Front Comput. Neurosci.*:10.
- [24] Jonsson J (2008), *Simplicial complexes of graphs*, Berlin; New York: Springer. xiv, 378 pp.
- [25] Sayer R, Friedlander M, Redman S (1990), The time course and amplitude of EPSPs evoked at synapses between pairs of CA3/CA1 neurons in the hippocampal slice, *J. Neurosci.*, 10: 826-836.
- [26] Mizuseki K, Sirota A, Pastalkova E, Buzsaki G (2009), Theta oscillations provide temporal windows for local circuit computation in the entorhinal-hippocampal loop, *Neuron* 64: 267-280.
- [27] Thompson LT, Best PJ (1990), Long-term stability of the place-field activity of single units recorded from the dorsal hippocampus of freely behaving rats, *Brain Res.* 509: 299-308.
- [28] McNaughton BL, Battaglia FP, Jensen O, Moser EI, Moser MB (2006), Path integration and the neural basis of the ‘cognitive map’, *Nat Rev. Neurosci.* 7: 663-678.
- [29] Shapiro M (2001), PLasticity, hippocampal place cells, and cognitive maps, *Arch Neurol.* 58: 874-881.
- [30] O’Reilly RC, McClelland JL (1994), Hippocampal conjunctive encoding, storage, and recall: Avoiding a trade-off, *Hippocampus* 4: 661-682.
- [31] Kuhl BA, Shah AT, DuBrow S, Wagner AD (2010) Resistance to forgetting associated with hippocampus-mediated reactivation during new learning, *Nat Neurosci.* 13: 501-506.
- [32] Murre JM, Chessa AG, Meeter M (2013) A mathematical model of forgetting and amnesia, *Frontiers in Psychology* 4.
- [33] Selkoe DJ (2002), Alzheimer’s Disease Is a Synaptic Failure, *Science* 298: 789-791.
- [34] Palop JJ, Chin J, Roberson ED, Wang J, Thwin MT, et al. (2007) Aberrant Excitatory Neuronal Activity and Compensatory Remodeling of Inhibitory Hippocampal Circuits in Mouse Models of Alzheimer’s Disease, *Neuron* 55: 697-711.
- [35] Cacucci F, Yi M, Wills TJ, Chapman P, O’Keefe J (2008) Place cell firing correlates with memory deficits and amyloid plaque burden in Tg2576 Alzheimer mouse model, *Proc. Natl. Acad. Sci.* 105: 7863-7868.
- [36] Busche MA, Konnerth A (2015), Neuronal hyperactivity-A key defect in Alzheimer’s disease? *Bioessays* 37: 624-632.
- [37] Busche MA, Eichhoff G, Adelsberger H, Abramowski D, Wiederhold K-H, et al. (2008). Clusters of Hyperactive Neurons Near Amyloid Plaques in a Mouse Model of Alzheimer’s Disease. *Science* 321: 1686-1689.
- [38] Busche MA, Chen X, Henning HA, Reichwald J, Staufenbiel M, et al. (2012). Critical role of soluble amyloid- β for early hippocampal hyperactivity in a mouse model of Alzheimer’s disease. *Proc. Natl. Acad. Sci.* 109: 8740-8745.
- [39] Minkeviciene, R., Rheims, S., Dobszay, M.B., Zilberter, M., Hartikainen, J., Fulop, L., Penke, B., Zilberter, Y., Harkany, T., Pitkanen, A., and Tanila, H. (2009). Amyloid beta-induced neuronal hyperexcitability triggers progressive epilepsy, *J Neurosci.* 29: 34533462.
- [40] Šišková Z, Justus D, Kaneko H, Friedrichs D, Henneberg N, et al. (2014) Dendritic Structural De-

- generation Is Functionally Linked to Cellular Hyperexcitability in a Mouse Model of Alzheimer's Disease. *Neuron* 84: 1023-1033.
- [41] Laxton AW, Tang-Wai DF, McAndrews MP, Zumsteg D, Wennberg R, et al. (2010). A phase I trial of deep brain stimulation of memory circuits in Alzheimer's disease. *Ann Neurol.* 68: 521-534.
- [42] Shirvalkar PR, Rapp PR, Shapiro ML (2010). Bidirectional changes to hippocampal theta-gamma comodulation predict memory for recent spatial episodes. *Proc. Natl. Acad. Sci.* 107: 7054-7059.
- [43] Babichev A, Dabaghian Y (2017), Transient cell assembly networks encode stable spatial memories. *Sci. Reports* 7: 3959.
- [44] McClelland JL, McNaughton BL, O'Reilly RC (1995). Why there are complementary learning systems in the hippocampus and neocortex: insights from the successes and failures of connectionist models of learning and memory. *Psychol Rev.* 102: 419-457.
- [45] Fusi S, Drew PJ, Abbott LF (2005). Cascade Models of Synaptically Stored Memories. *Neuron* 45: 599-611.
- [46] Barbieri R, Frank LM, Nguyen DP, Quirk MC, Solo V, et al. (2004). Dynamic analyses of information encoding in neural ensembles. *Neural Comput.* 16: 277-307.
- [47] Buzsaki G (2005). Theta rhythm of navigation: link between path integration and landmark navigation, episodic and semantic memory. *Hippocampus* 15: 827-840.
- [48] Fu H, Rodriguez GA, Herman M, Emrani S, Nahmani E, et al., (2017) Tau Pathology Induces Excitatory Neuron Loss, Grid Cell Dysfunction, and Spatial Memory Deficits Reminiscent of Early Alzheimer's Disease. *Neuron* 93: 533-541.e535.
- [49] Persson P-O, Strang G (2004), A simple mesh generator in MATLAB, *SIAM Review* 46: 329-345.

VIII. SUPPLEMENTARY FIGURES

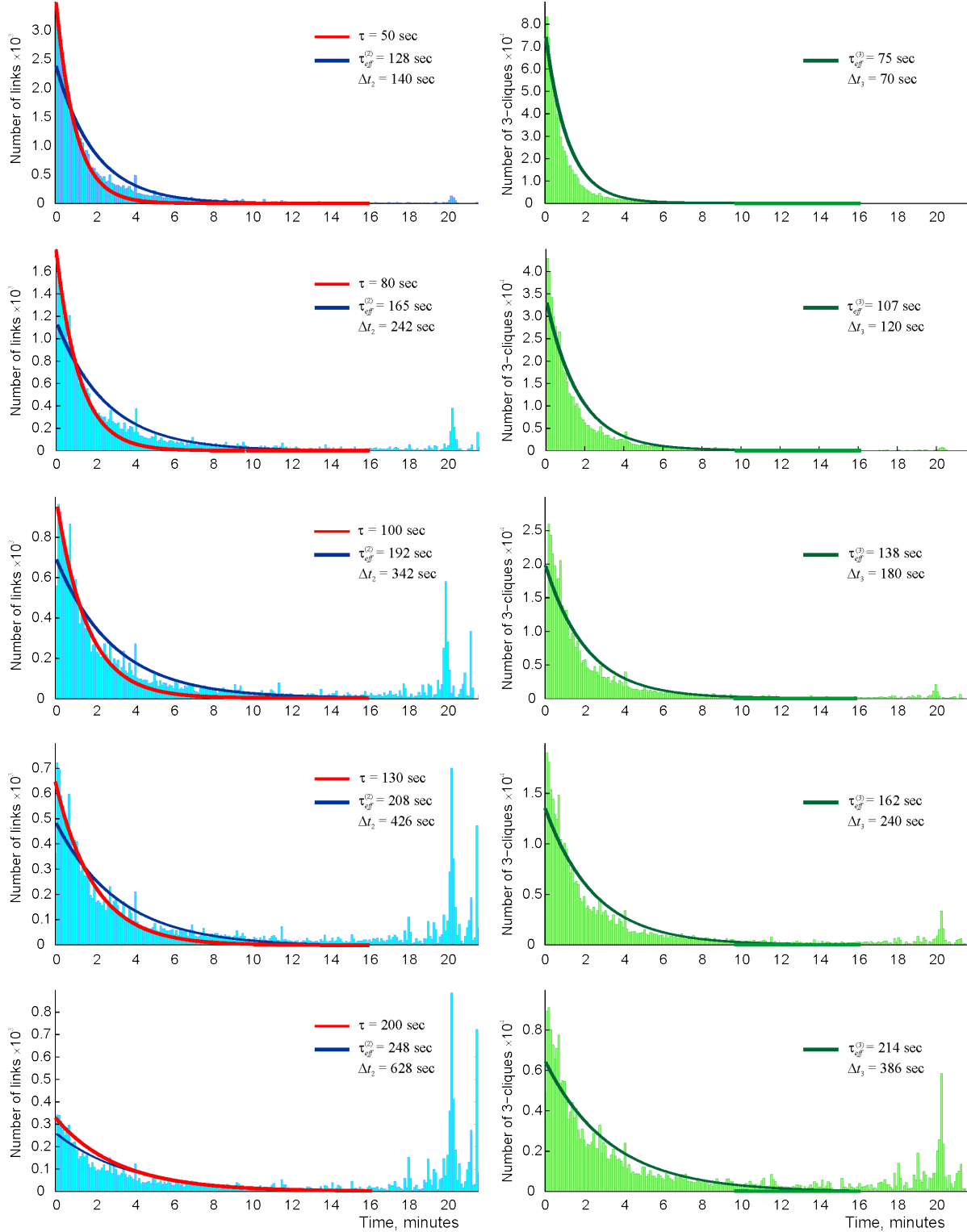


FIG. S1: **Statistics of the connections' lifetimes.** A: Histograms of the intervals between consecutive births (b) and deaths (d) of the pairwise ($\Delta t_{s_i^2} = t_{s_2}^{(d_i)} - t_{s_2}^{(b_i)}$, left column of panels) and triple ($\Delta t_{s_i^3} = t_{s_3}^{(d_i)} - t_{s_3}^{(b_i)}$, right column of panels) connections, for five values of the proper decay times τ . The red line outlines the exponentials with proper decay time $1/\tau$ and the dark-blue line shows the exponential fit of the histogram with the decay rate $1/\tau_e$, computed for the under 16 mins long intervals. The exponential fit to the histogram of the effective lifetimes of short-living triple connections ($\Delta t_{s_i^3} < 10$ mins) is shown by dark-green line on the right panels. The mean lifetime for the entire population of links, Δt_k , is shown at the on each panel.

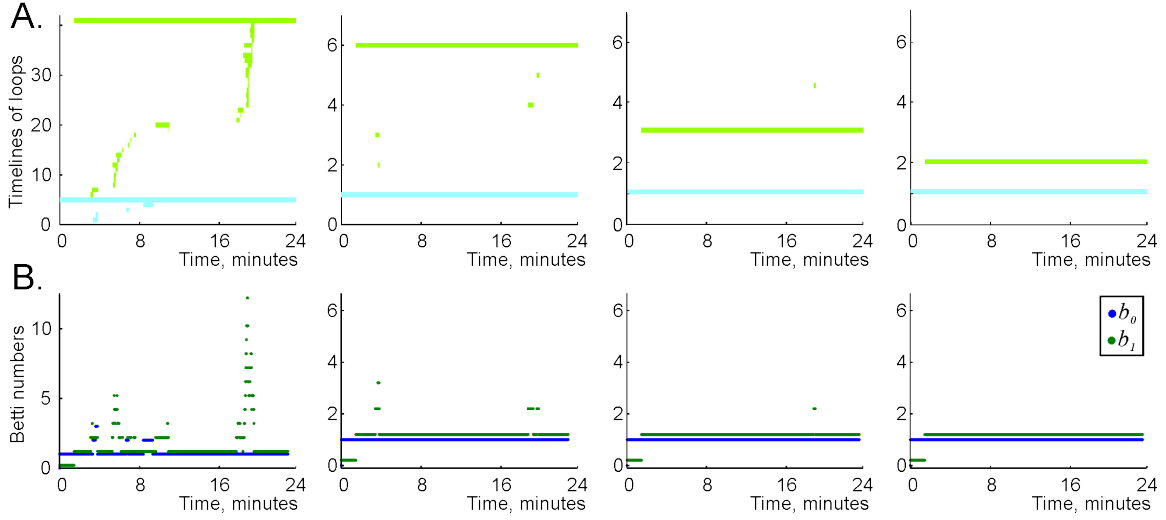


FIG. S2: **Longer decay times suppress topological instabilities.** A: Timelines of 0D (light-blue) and 1D (light-green) topological loops in the flickering coactivity complex, computed for four values of the proper decay time τ . B: The corresponding Betti numbers, $b_0(\mathcal{F}_\tau)$ (blue) and $b_1(\mathcal{F}_\tau)$ (green).

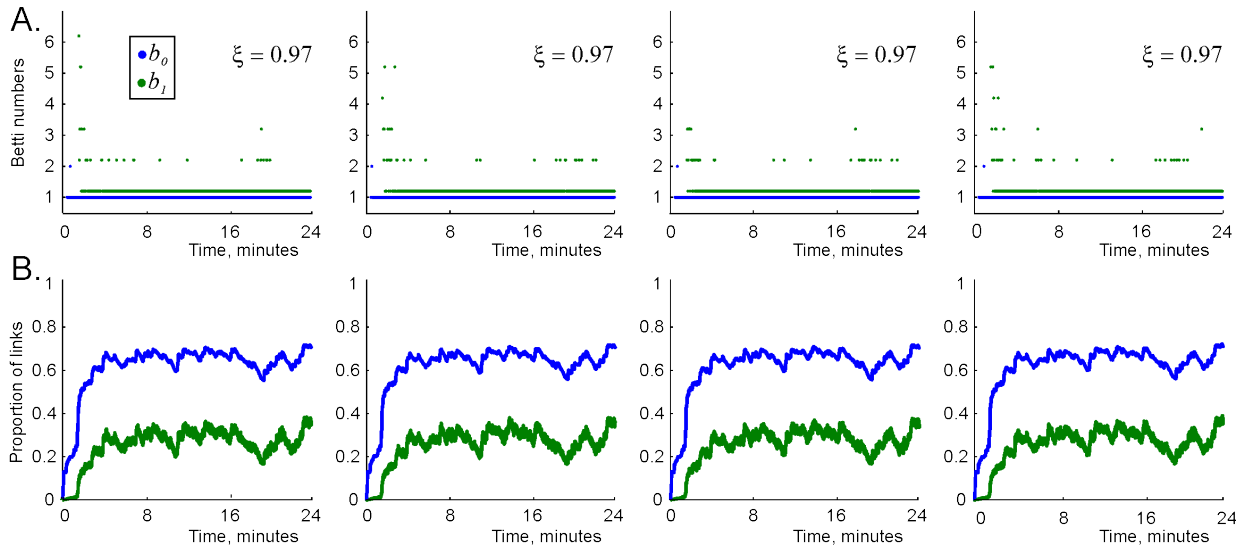


FIG. S3: **Topological properties of the random complex.** A. Four tests of the topological behavior of the random complex \mathcal{F}_r indicate that after initial period of about 3 minutes, this complex produces occasional one-dimensional topological loops in only 3% of the time (success rate $\xi = 0.97$ in all cases). B. The numbers of double and triple connection remains approximately the same from case to case.

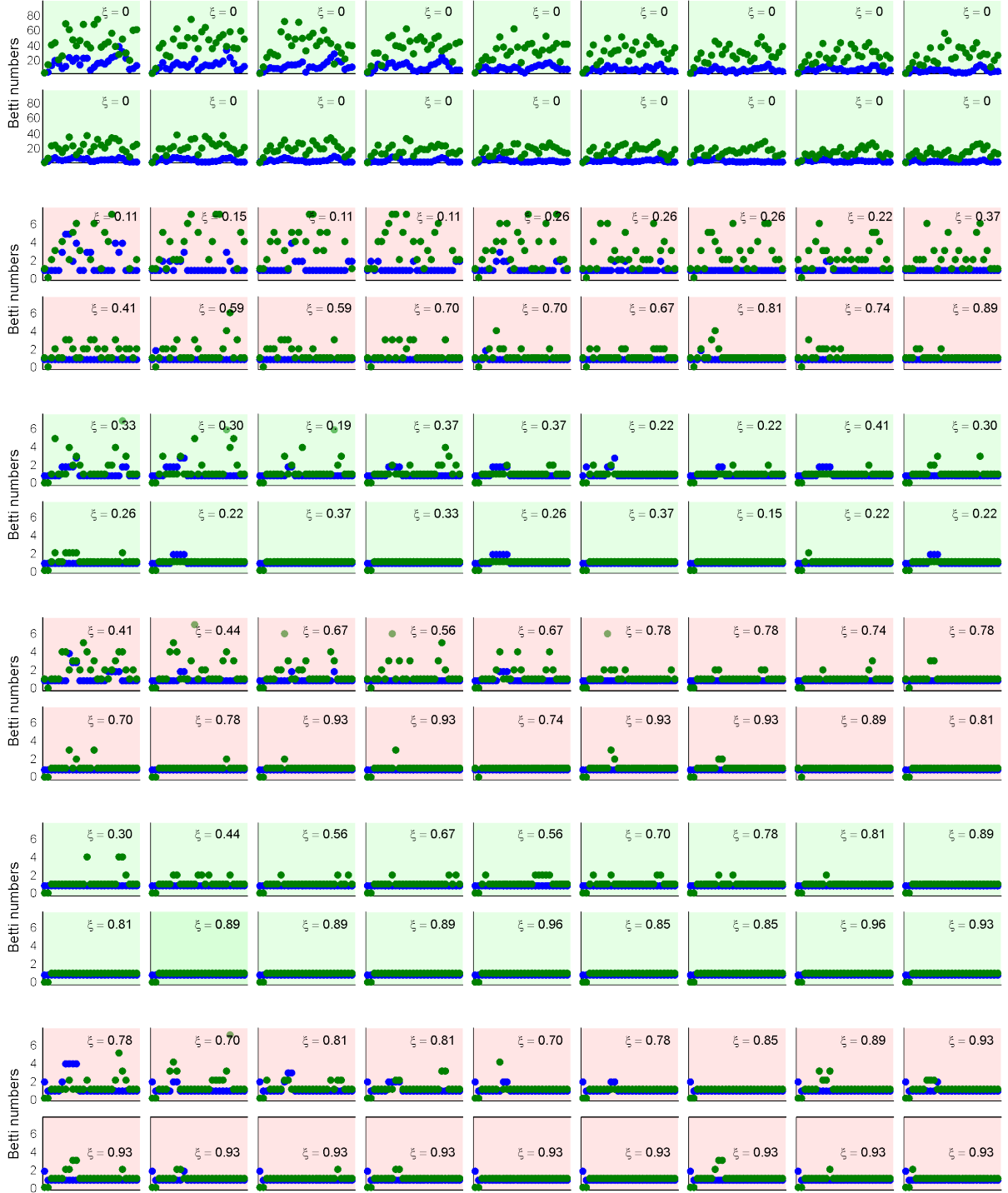


FIG. S4: **Suppression of topological fluctuations by increasing place cell firing rates.** The six consecutive pairs of rows (colors alternate for illustrative purposes) correspond to the ensemble mean firing rate $f = 12, 14, 16, 18, 20$ and 24 Hz. The proper decay time increases along each pair of rows from $\tau = 75$ to $\tau = 200$ secs, uniformly across the intermediate values. As τ increases, the percentage of times (ξ) during which the Betti numbers $b_k(\mathcal{F}_\tau)$, $k = 0, 1$, remain equal to their physical values increases, for all ensemble mean firing rates. The higher is the ensemble mean frequency rate, the smaller are the topological fluctuations across the entire range of τ s.